JOURNAL OF MATERIALS SCIENCE **38** (2003) 1063–1071

Mechanical behavior of glass polymer multilayer composites

A. SEAL, S. K. DALUI, A. K. MUKHOPADHYAY*, K. K. PHANI, H. S. MAITI
Central Glass and Ceramic Research Institute, Calcutta 700 032, India
E-mail: anoopmukherjee@rediffmail.com

To identify the best reinforcement condition for development of tough glass polymer multi-layer composites (GPMLC) with high failure strain, two such model composite structures were developed. Soda–lime–silica glasses of two different thicknesses viz (A—1.01 mm and B—1.17 mm) were used as the matrix layers. The A-glass and B-glass based GPMLC samples were prepared by a novel, low pressure lamination technique applied to the alternating planar structure of the matrix and reinforcing phases. These GPMLC materials were fabricated with and without a thin sprayed layer of kerosene, between the glass layer and the reinforcing layer in the interface where; the interface was either epoxy (a thermosetting resin) or polyvinyl butyral (PVB, a thermoplastic resin). The GPMLC samples which exhibited stepped load—displacement behaviour in the most pronounced fashion, had the thermoplastic resin at the interface. Most of these GPMLC samples had a thin layer of kerosene intentionally introduced between the glass layer and the reinforcing polymer layer such that a weak interface is obtained. Fractographic evidence suggested that more of controlled delaminaton cracking occurs in such samples. Apart from the chemical nature of the reinforcing polymer phase, the interfacial layer thickness (h_i) and the interfacial shear stress (τ_{xy}) were found out to have significant influence on the specific failure load and the failure stress of the current glass polymer multi-layer composites.

1. Introduction

Monolithic ceramic materials fail by brittle failure from pre-existing flaws. The approach to fabricate particulate or fibre reinforced ceramic matrix composite (CMC) was developed to counter this problem. However, the high cost of processing, lack of control over the dispersion of the reinforcing phase in the microstructure and health-hazard associated with fine fibres e.g. whiskers, has led to the development of multi-layer ceramic composites (MLC).

In MLC a flexible design philosophy can be adopted to tailor the microstructure layer by layer to suit a predetermined end application. The thermal expansion mismatch between layers of dissimilar materials and the bonding quality at the interface are the two key factors which govern the property of MLC. Most of the studies have been devoted to multi-layered ceramic materials such as Alumina/Zirconia [1], Alumina/Titanium Carbide/($MoSi_2 + Mo_2B_5$) [2], Silicon Carbide/Graphite [3], Silicon Nitride/Boron Nitride [4], Alumina/$LaPO_4$ [5] etc. systems with either weak or strong interfacial bonding. In fact, a recent theoretical model [6] suggests that high failure strain can be attained in MLCs if the interface between the layers is sufficiently strong to prevent sliding but has a fracture resistance low enough to induce in plane crack deflection.

However, there has been very little experimental study on mechanical behaviour of glass polymer multilayer composites (GPMLC). In the lone example, multiple layers of indented glass slides or unindented cover slips were used with a thermoplastic adhesive to fabricate hot pressed GPMLC [7]. The mechanical behaviour of such a system was found to be in somewhat qualitative agreement with the theoretical predictions [6].

The present authors have already shown that significant enhancement of specific failure load and load point displacement at failure can be attained in glass-polymer laminar composites by suitable choice of the type and amount of the reinforcing phase [8–10]. Use of various reinforcements have led to significant enhancement in displacements to failure along with the exhibition of fibre reinforced composite—like stress strain behaviour [8, 9]. It has been demonstrated further, that the presence of a thin, sprayed layer of kerosene between the glass and epoxy layers can induce significant extent of controlled, localised debonding that might affect better accomodation of applied strain [10]. The objective of the present study was to fabricate and characterize

*Author to whom all correspondence should be addressed.

GPMLC with varying interface properties. In addition, an attempt was made to compare experimentally observed stress-strain behaviour of GPMLC with the behaviour predicted according to the theoretical model [6].

2. Experimental

Unindented, annealed soda-lime-silica glass slides of two different thickness 1.01 ± 0.01 mm (type A) and 1.17 ± 0.02 mm (type B) were used as the matrix layers for fabrication of the GPMLC samples. The typical chemical analysis data of the soda lime silica glasses are given in Table I. Mechanical properties data of the soda lime silica glasses are presented in Table II.

In fabricating the multi-layer composite (MLC) samples, the reinforcing polymer layer comprised of either a thermosetting adhesive [Araldite Epoxy Resin, LY 556 (Ciba Speciality Chemicals (India) Ltd.] with 15–20% hardener HY 951 [Cibatul Ltd., India] or a thermoplastic adhesive [Polyvinyl Butyral (PVB), Hipol B-30, Molecular Weight ~72,000; Parekh Chemicals, India]. This was done intentionally to have variable interface layer properties in the GPMLC. Accordingly, the GPMLC samples are termed as AE (A-glass-epoxy MLC), AP (A-glass-PVB MLC), BE(B-glass-epoxy MLC) and BP (B-glass-PVB MLC).

For both types of glasses (A, B) and adhesives [Epoxy (E) or PVB (P)], additional GPMLC samples were prepared with a thin, mechanically sprayed interfacial kerosene layer between the glass and the adhesive layer so that a weak interfacial bonding is promoted. Accordingly these specimens are termed as A (E+K) [A-glass-epoxy-kerosene MLC], A (P+K) [A-glass-PVB-kerosene MLC], B(E+K) [B-glass-epoxy-kerosene MLC] and B(P+K) [B-glass-PVB kerosene MLC]. This was done on the basis of previous experience [10] that a thin kerosene layer between the matrix glass and the reinforcing epoxy layer can promote significant extent of controlled debonding. All GPMLC samples were fabricated by alternate placement of glass (A, B) and the reinforcing phase (Epoxy or PVB) by a hand lay up technique followed by lamination at a low pressure of 2–5 kPa [8–10] and a temperature of either 20–50°C (E/E+K system) or 130°C–150°C (P/P+K system).

Further, for all GPMLC structure the architecture was a combination of three glass slides with two interface layers placed alternately, as shown schematically in Fig. 1. The two outermost layers were kept always as glass. The density (ρ) of the samples was measured gravimetrically. The volume percent of the reinforcing phase (V_f) was measured from the difference of weight taken before and after burning out the respective adhesives and the sample dimensions of the GPMLC samples. The interface layer thickness (h_i) and the total sample thickness (h_t) were measured by a optical microscope and the accuracy of the measurement was found out to be within $\approx \pm 2.05\ \mu$m as checked out with scanning electron microscopic observations [8–10].

All samples were tested under the laboratory humidity condition and at a temperature of 30°C by conventional 3-point bend test in a universal testing machine (Instron 5500R) with a cross head speed (CHS) of 1 mm min^{-1}. The span length (L) was 60 mm. The load point displacement (δ) at failure was monitored by a linear variable differential transformer (LVDT). The LVDT had a sensitivity of 0.7% of the full scale deflection For all the tests a load cell of 1 KN was used with a machine resolution of ±5 N.

All reported data comprised of the average value of at least 5 to 10 individual tests. The error bars included in some of the figures represent ±1 standard deviation. The failure stress (σ_f), Young's Modulus (E) and failure strain (ε) of all samples were measured following equations of beam theory [3, 6, 7, 11]. The experimental values of the normalized stress and strain of the composites are calculated by normalizing with respect to the data of the corresponding glass matrices (A, B).

The interfacial shear stress (τ_{xy}) was estimated by the following equation [11]:

$$\tau_{xy} = \frac{3P}{bt^3}\left[\frac{t^2}{4} - y_1^2\right] \quad (1)$$

TABLE I Chemical compositions of A and B type glasses

Constituent (wt%)	Glass type A	Glass type B
SiO_2	69.35	71.68
Al_2O_3	2.40	2.07
Fe_2O_3	0.10	0.10
CaO	7.57	6.72
MgO	4.70	4.09
K_2O	1.49	1.63
Na_2O	14.32	13.56
TiO_2	Traces	Traces

TABLE II Physical and mechanical properties of A and B type glasses

Properties	Glass type A	Glass type B
Density (gm/cc)	2.36 ± 0.11	2.53 ± 0.13
Thickness (mm)	1.01 ± 0.01	1.17 ± 0.02
Young's modulus[a], E (GPa)	73.86 ± 2.86	75.90 ± 2.80
Flexural strength[b] (MPa)	77.01 ± 13.10	74.95 ± 13.87
Vicker's microhardness[c], H (GPa)	4.50 ± 0.17	4.60 ± 0.21
Fracture toughness[d] K_{IC} (MPa . $m^{0.5}$)	0.89 ± 0.05	0.87 ± 0.03

[a]Measured by static beam bending method.
[b]Measured by 3-point bend strength with a span of 60 mm, CHS = 1 mm/min.
[c]Measured with applied load (P) of 10 N–20 N (load independent hardness regime).
[d]Measured by indentation technique at $P = 20$ N [8–10, 12].

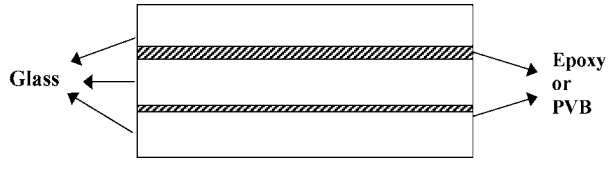

Figure 1 Schematic presentation of GPMLC sample fabrication architecture.

where, P is the applied load, t is sample thickness, y_1 is depth of the layer from the neutral axis in which the shear stress is calculated and b is width of the sample.

The indentation fracture toughness (K_{ic}) data of the matrix glasses (Table II) were measured following [12]. For the purpose of fractographic investigations, an ordinary optical microscope was employed to obtain top view and side view stereophotomicrographs of all the GPMLC samples to identify the process of failure initiation and crack propagation. The advantage with the optical microscopy technique used here is that the internal reflections off the crack surface can take place. This is manifested as discontinuous regions of brightness in the photomicrographs.

3. Results

3.1. Mechanical behaviour of the composites

The data on mechanical behaviour of the A-glass based GPMLC (A-GPMLC) and the B-glass based GPMLC (B-GPMLC) samples are presented in Figs 2–15. Both the quantities volume percent of the reinforcing phase, V_r (%) and failure load per unit thickness (P_f / h_t) of A-GPMLC samples decreased with density (ρ) (Fig. 2). The density and the specific failure of A-GPMLC samples were much higher than those of the matrix (A-glass, density—2.36 gm/cc).

Similarly, the volume percent of the reinforcing phase, V_r (%), of the B-GPMLC samples generally decreased with density, except for B(P) (Fig. 3). However, in general, the density of the B-GPMLC samples was lower than that of the B-glass matrix (2.53 gm/cc). The B-GPMLC samples had specific failure load much higher than that of B-glass.

The typical data on load (P) vs. load-point displacement (δ) patterns of both A- and B-GPMLC samples are shown in Figs 4 and 5. The data indicate a stepped load unload behaviour akin to that of fibre reinforced ceramic matrix composites (CMC).

Normalized stress strain data of both A- and B-GPMLC samples are shown in Figs 6 and 7. In both

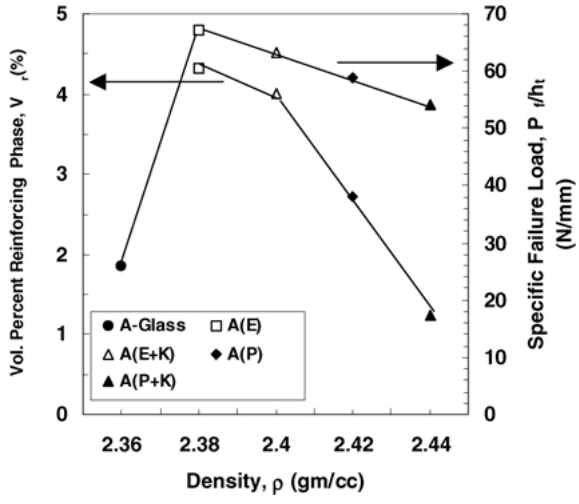

Figure 2 Variation of volume percent reinforcing phase and specific failure load with density (ρ) of A-GPMLC samples.

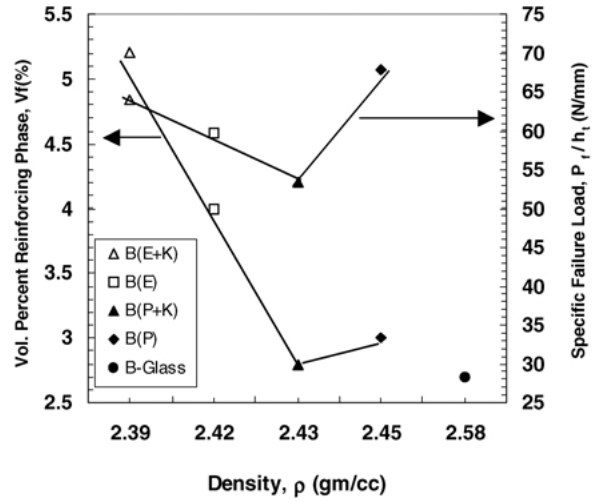

Figure 3 Variation of volume percent reinforcing phase and specific failure load with density (ρ) of B-GPMLC samples.

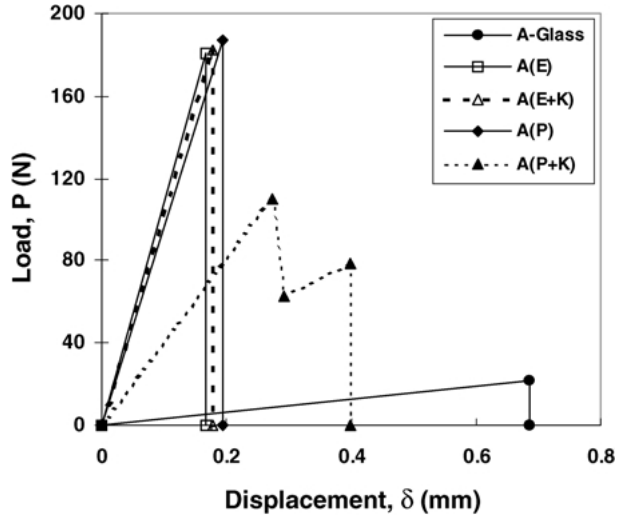

Figure 4 Stepped load-displacement behaviour of A-GPMLC samples.

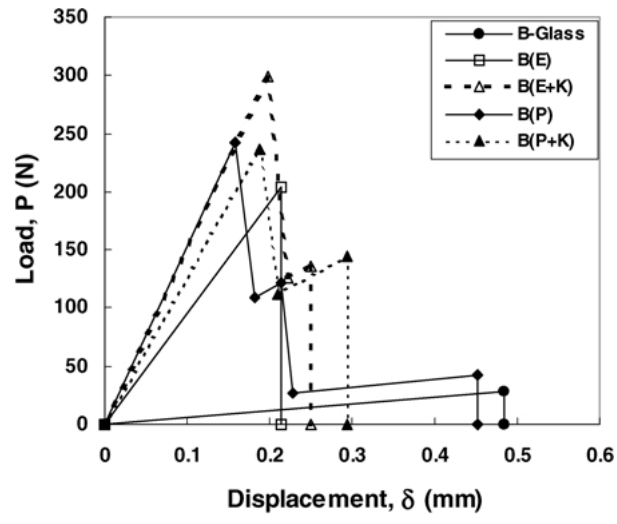

Figure 5 Stepped load-displacement behaviour of B-GPMLC samples.

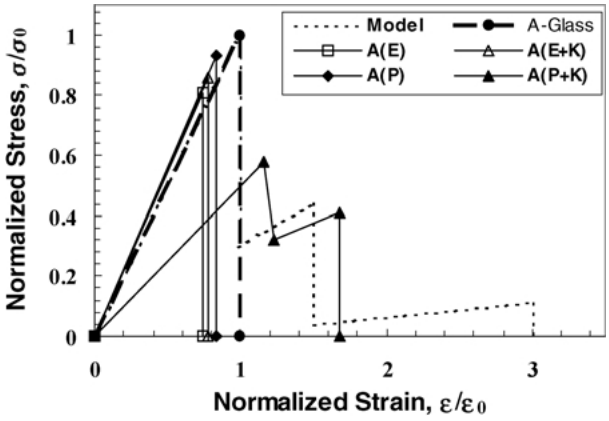

Figure 6 Normalized stress-strain behaviour of A-GPMLC samples.

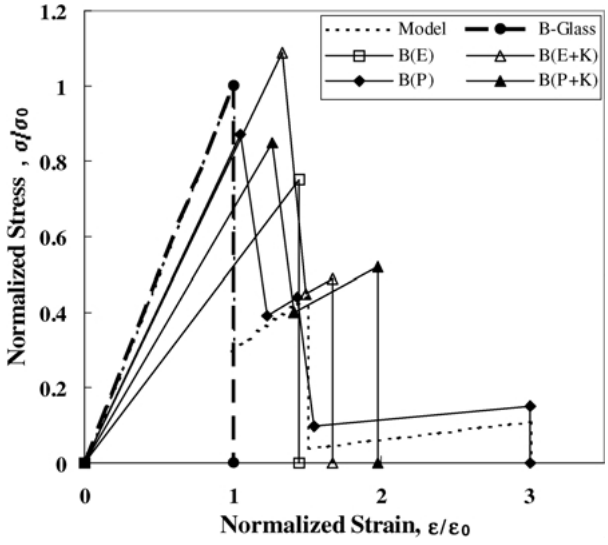

Figure 7 Normalized stress-strain behaviour of B-GPMLC samples.

these figures, the predicted behaviour according to the theoretical model [6] are included as dotted lines, for the purpose of comparison only. The present experimental data do not completely match with the predicted pattern although there is some qualitative agreement.

In the case of A-GPMLC samples the interface layer thickness (h_i) and failure stress (σ_f) decreased with density, Fig. 8. The normalized stress and specific failure load showed a strong dependence on interface layer thickness (h_i) of A-GPMLC samples, Fig. 9. The Young's modulus (E) and the failure strain data of the A-GPMLC samples also generally increased with the interfacial layer thickness, Figs 10 and 11.

However, in the case of B-GPMLC samples although the interfacial layer thickness (h_i) decreased with density but the failure stress (σ_f) showed a somewhat opposite trend, Fig. 12a and b. The specific failure load (P_f / h_t) and normalized stress increased with the theoretically estimated value of interfacial shear stress (τ_{xy}), Fig. 13.

Generally, the Young's modulus (E) increased with interfacial layer thickness (Fig. 14) but the failure strain (ε) decreased with the estimated interfacial shear stress (τ_{xy}) of the B-GPMLC samples, Fig. 15.

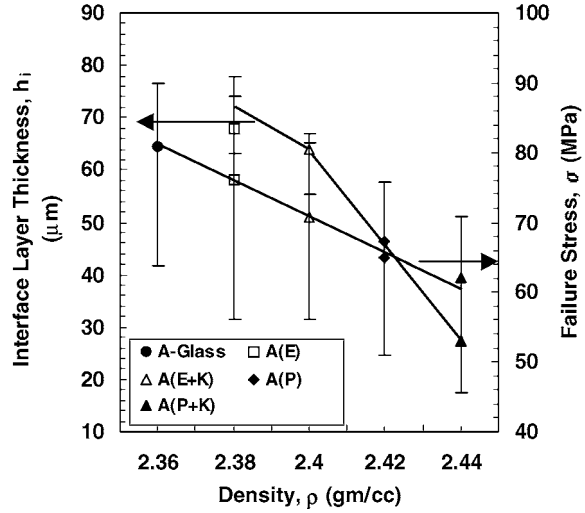

Figure 8 Variation of interfacial layer thickness and failure stress with density (ρ) of A-GPMLC samples.

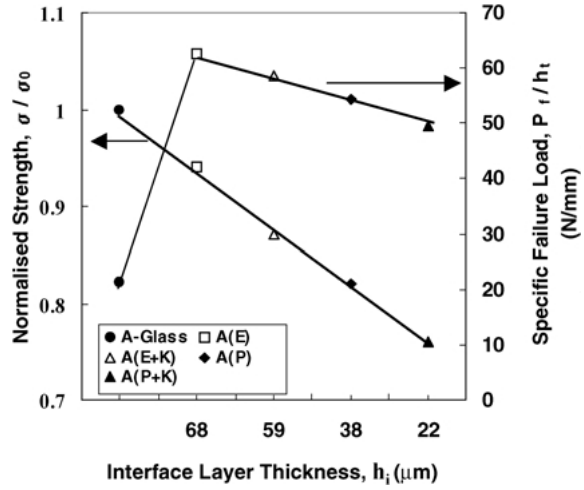

Figure 9 Variation of normalized stress and specific failure load with interfacial layer thickness of A-GPMLC samples.

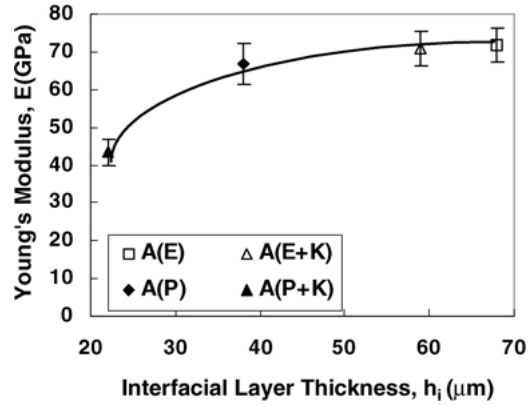

Figure 10 Young's modulus vs. interfacial layer thickness of A-GPMLC samples.

3.2. Fractography

The results of the fractographic studies on the present GPMLC samples are shown in Fig. 16a–e. The typical initiation point was always from a major crack at the tensile surface of the GPMLC sample, for instance, as shown here for the sample A(E+K), Fig. 16a. The

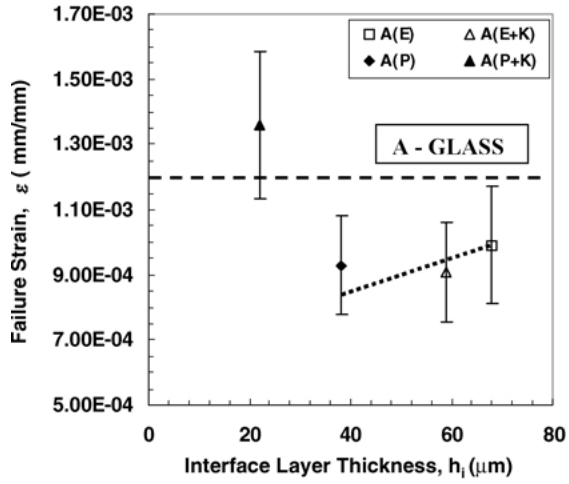

Figure 11 Failure strain vs. interfacial layer thickness of A-GPMLC samples.

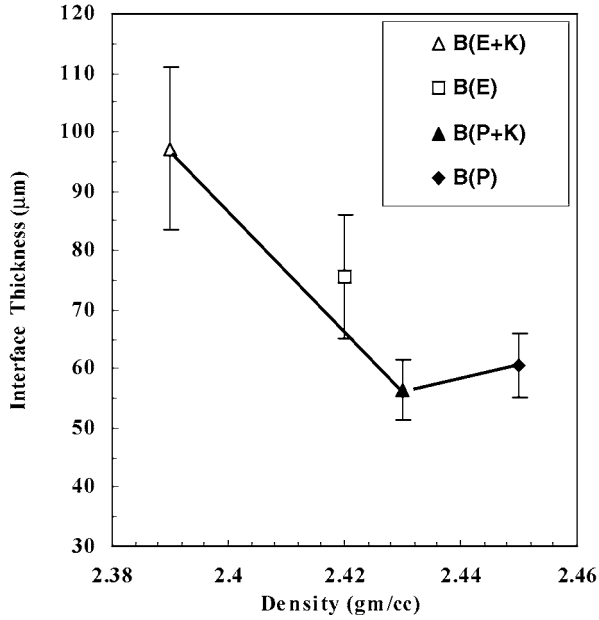

(a)

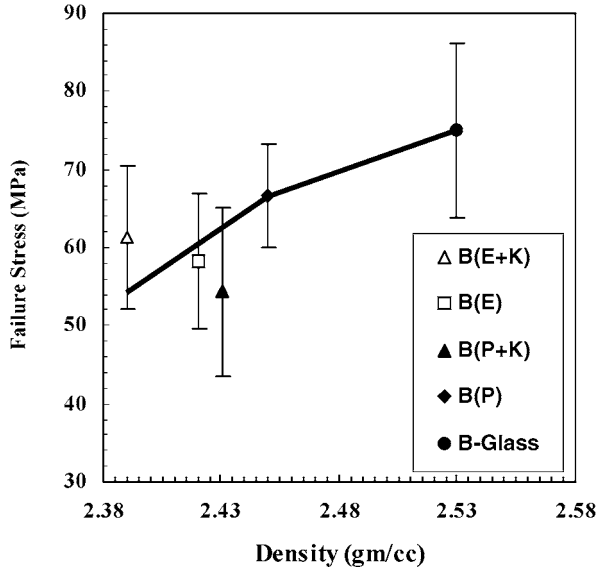

(b)

Figure 12 (a) Variation of interfacial layer thickness of B-GPMLC samples with density. (b) Variation of failure stress of B-GPMLC samples with density.

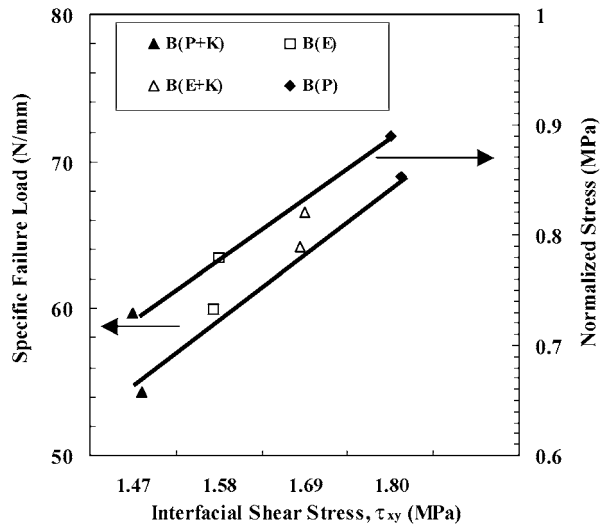

Figure 13 Specific failure load and normalized stress vs. interfacial shear stress of B-GPMLC samples.

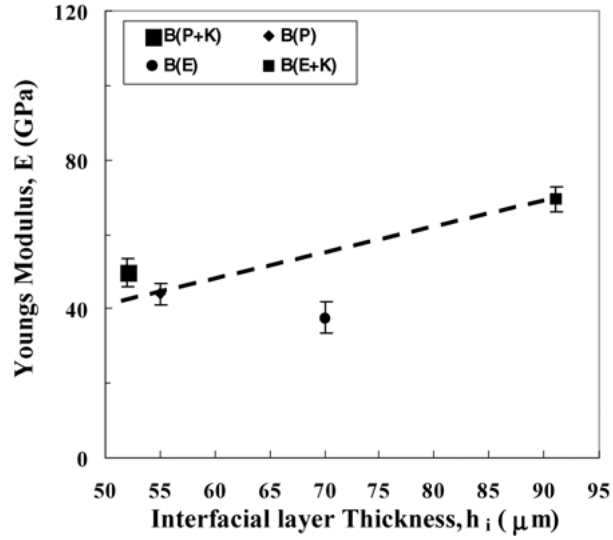

Figure 14 Young's modulus vs. interfacial layer thickness of B-GPMLC samples.

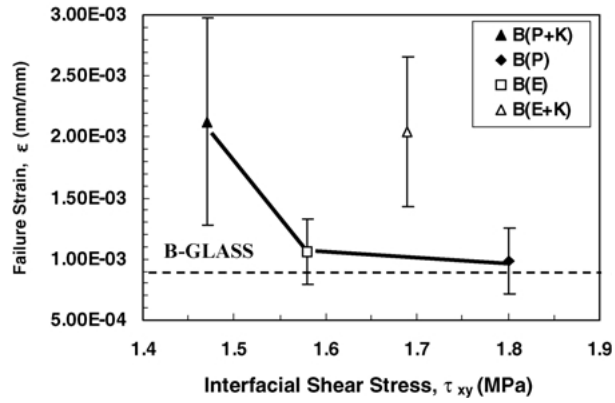

Figure 15 Failure strain vs. interfacial shear stress of B-GPMLC samples.

(a)

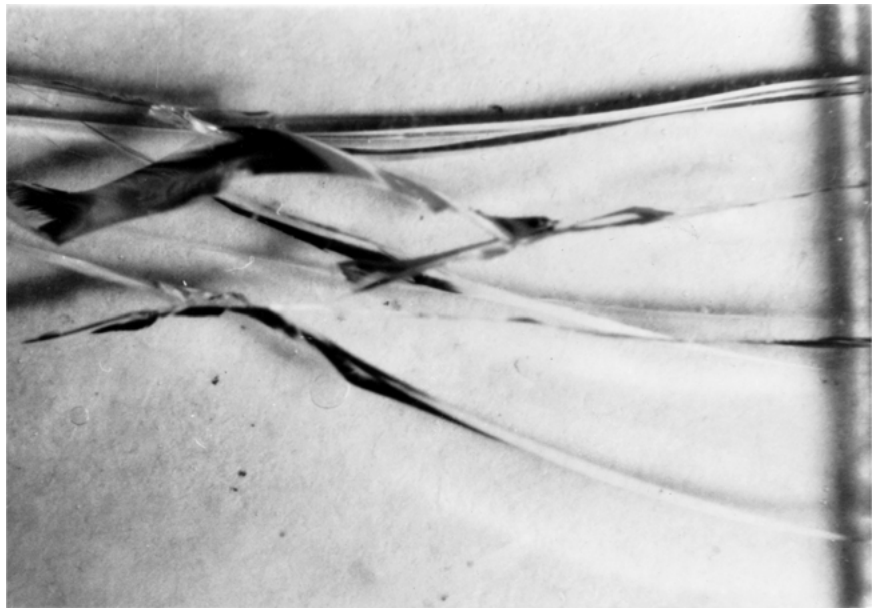

(b)

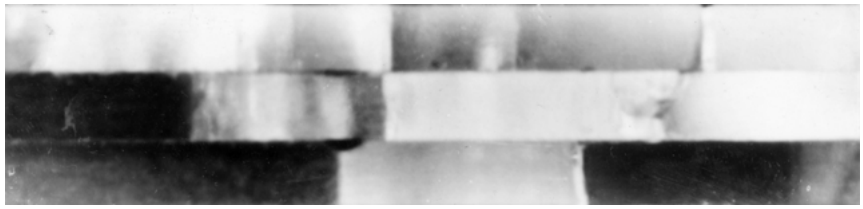

(c)

(d)

(e)

Figure 16 (a) Side view of crack propagation in GPMLC sample A(E+K). (b) Top view of typical crack branching in GPMLC sample B(E). (c) Side view of crack propagation in GPMLC sample B (P). (d) Side view of crack propagation in GPMLC sample B (E). (e) Side view of crack propagation in GPMLC sample B (E+K) (T-Tensile Side).

process of crack propagation characteristically involved multiple crack branching as shown in the typical example for the GPMLC sample B(E), Fig. 16b.

However, the extent of delamination cracking was much more for polyvinyl butyral based polymeric interface (sample B(P), Fig. 16c) than for the epoxy based polymeric interface (sample B(E), Fig. 16d). The extent of delamination cracking was further enhanced in presence of the thin kerosene layer (sample B(E+K), Fig. 16e).

4. Discussions

Based on the current experimental results (Figs 2–16), the following general comments can be made. Generally all GPMLC samples have lower fracture strength

values than those of the corresponding glass matrices. Of all A-GPMLC materials, A(E) exhibits the highest failure stress. Similarly, B(P) exhibits the highest failure stress among B-GPMLC samples.

However, the failure strain was highest for the samples A(P+K) and B(P+K) in their respective categories. All GPMLC samples taken together, the failure stress was highest for the A(E) samples. But the highest value of the failure strain was obtained for the B(P+K) samples.

Among the four samples A(P+K), B(E+K), B(P) and B(P+K) which exhibited MLC like stepped load-displacement behaviour in the most pronounced fashion, three samples have the polyvinyl butyral resin as one component of the phase present at the interface between the adjacent glass layers. All three of these samples i.e. A(P+K), B(E+K) and B(P+K) had a thin layer of kerosene intentionally introduced between the glass layer and the reinforcing polymer layer such that a weak interface is obtained. Such a weak interface might have promoted controlled, localized debonding that affect more in-plane crack deflection and hence may induce more fracture energy absorption [3, 6, 7].

For the present GPMLC samples, the failure stress (σ_f) is given by,

$$\sigma_f = \frac{1}{Y}\left(K_{\mathrm{IC}}^{\mathrm{eff}}\right) \cdot (a_{\mathrm{cg}})^{-0.5} \tag{2}$$

Here, Y is a constant for the three point bend loading configuration employed in the present work and a_{cg} can be treated as a characteristic flaw size parameter because the crack initiates always at the glass surface, Fig. 16b. Under such conditions, the failure stress is dictated by the effective toughness of the composite material.

The data obtained in the present work clearly demonstrate that the interfacial layer thickness (h_i) and the interfacial shear stress (τ_{xy}) can have significant influence on the failure stress of the glass polymer multi-layer composite. Unfortunately, the available models [6, 13] do not take these factors into account.

From the experimental observations of stepped load-unload behaviour in the load-displacement plot (Figs 4 and 5) and the fractographic evidence (Fig. 16a–16e), it is evident that the extent of controlled debonding at the interface actually plays the key role to affect the failure process of these composites. To the best of our knowledge no analytical expression is available for calculating the interfacial delamination failure energy (γ_{fi}) of multi-layered glass polymer laminar composites. Therefore, following the work of Mawdsley *et al.* [5] who measured the delamination fracture energy of alumina-monazite multilayer composites; we suggest the following approximate expression for (γ_{fi}):

$$\gamma_{\mathrm{fi}} \cong \left[\frac{3 \cdot P_{\mathrm{cd}}^2 \cdot L^2\left(1-\nu_g^2\right)}{2 \cdot E_g (h_g + h_i)^3 b^2}\right]\left[\left(\frac{h_g}{h_i}+1\right)^3 - 1\right] \tag{3}$$

In expression (3) , P_{cd} represents the critical load at which debonding initiates, L is the span length in the three point bend test, ν_g is the Poisson's ratio of glass, E_g is the Young's modulus of glass, h_g is the thickness of the glass layer, h_i is the thickness of the interface layer and b is the width of the glass slide. Rearranging Equation 3, bearing in mind that for the present experimental glass polymer composites, typically $h_i / h_g \sim 0.018$ such that $(h_i + h_g)^{-3} \langle\langle (h_i)^{-3}$, we arrive at a simplified expression:

$$\gamma_{\mathrm{fi}} \approx [A] \cdot h_i^{-3} \tag{4}$$

where, the quantity A is a parameter to be determined experimentally.

The quantity A is given by the following expression:

$$A = \left[\frac{3 \cdot P_{cd}^2 \cdot L^2\left(1-\nu_g^2\right)}{2 \cdot E_g b^2}\right] \tag{5}$$

The significance of Equation 4 is only that it relates the effective interfacial delamination failure energy to the interfacial layer thickness. Assuming that for a given glass polymer multi-layer composite system under a three point flexural loading pattern, quantities like L (loading span), ν_g (Poisson's ratio of glass), E_g (Young's modulus of the matrix glass phase), b (the width of the matrix glass slides) and P_{cd} (critical load for debonding at the interface to initiate) remain constant, the crux of the message that the proposed Equation 4 conveys is that the interfacial delamination failure energy bears a very strong inverse dependence on the interfacial layer thickness.

Since P_{cd} is not exactly experimentally measured in the current results, a direct calculation of the γ_{fi} values is beyond the scope of the present work. However, the Equation 4 conveys a very important, yet simple message. For a given experimental loading configuration and glass matrix layer; the smaller is the interfacial layer thickness, the higher is the energy requirement for delamination cracking to occur. Conversely, for a thicker interface layer, lesser energy shall be required for the delamination cracks to grow along the interface. Similar observations have been reported by others [3, 13].

Now, assuming the principle of superposition, the total effective fracture toughness/failure resistance of the composite $(K_{\mathrm{Ic}})^{\mathrm{eff}}$ is given by

$$(K_{\mathrm{Ic}})^{\mathrm{eff}} = (K_{\mathrm{Ic}})_g + (K_{\mathrm{Ic}})_{\mathrm{fi}} \ \ldots\ldots\ldots \tag{6}$$

Here $(K_{\mathrm{Ic}})_g$ represents the constant contribution from the glass matrix and $(K_{\mathrm{Ic}})_{\mathrm{fi}}$ signifies the contribution from the interface layer.

It is suggested that $(K_{\mathrm{Ic}})_{\mathrm{fi}}$ will be more for composites with thicker interface layer. The reason is that as the energy requirement for delamination cracking to occur is lower, more of such cracking can take place and in the process cause more energy dissipation, thus leading to a rise in fracture toughness. On the other hands, for composites with thinner interface, since the energy requirement for delamination cracking to occur is much higher, the formation of such cracks become energetically less favourable. That means lesser amount of delamination cracking can take place here. Such a

situation leads to lesser amount of energy dissipation and hence, to a overall lower intrinsic toughness. If this conjecture is correct, the failure stress should be lower for the GPMLC with lower interface layer thickness and higher for higher interface layer thickness simply because the effective toughness controls the failure stress according to Equation 2. The experimental data on A-GPMLC (Fig. 9) fit into this scenario.

Now, keeping in mind that the neutral axis of the current experimental samples is at a distance of $[{}^1/_2(3h_g + 2h_i)]$ from the tensile surface, the relationship between the specific failure load (P_f/h_t) and the interfacial shear stress can be expressed as [11]:

$$(P_f/h_t) = \frac{b \cdot \tau_{xy}}{3h_g\left[\frac{1}{(3h_g+2h_i)} - \frac{h_g}{(3h_g+2h_i)^2}\right]} \tag{7}$$

Thus, for the purpose of simplification, neglecting terms higher than the first order in denominator, we obtain the following approximate expression:

$$(P_f/h_t) \cong \tau_{xy}\left[1 + \frac{2 \cdot h_i}{3 \cdot h_g}\right] \cdot b \tag{8}$$

It follows from Equation 8 that for a given sample with a given glass layer thickness (h_g) and a given interface layer thickness (h_i); the specific failure load should increase with enhancement in τ_{xy}. The present experimental data for B-GPMLC samples follow this trend (Fig. 13).

According to Equation 8, the specific failure load also can increase with enhancement in the interface layer thickness for a given GPMLC sample of width (b), as was indeed the data for A-GPMLC samples (Fig. 9).

A comparison of the photomicrographs presented in Fig. 16a–16e and the load-displacement patterns (Figs 4 and 5) suggest the following general, simplistic picture of failure process in the present GPMLC samples. The crack initiates at the tensile surface of the outermost glass layer. On initial loading, the crack grows perpendicular to the direction of the tensile stress (Fig. 16a). As the first outermost layer cracks, the through-the-thickness crack reaches the interface and turns parallel to the interface to affect delamination cracking (Fig 16a, and c). This can happen because of the low interfacial fracture toughness of the thin polymeric layer ($\approx$0.3–0.5 MPa $\cdot$ m$^{1/2}$, Ref. 14) in comparison to that of the thick glass layer ($\approx$0.8–1.1 MPa $\cdot$ m$^{1/2}$, Refs. 6, 8–10, 13).

As the interface fails to support further loading due the local delamination, the second glass layer starts to get loaded and sequentially a through the thickness crack develops across this layer (Figs 4 and 5 and 16a–c). This leads the crack to the next interface. Here, delamination cracking takes place again along the interface. The delamination crack continues to grow until the interfacial thin polymer layer fails to support further loading due to the local debonding that this crack causes. This crack propagation process leads finally to the loading of the third, outermost glass layer which ultimately fails as a through-the-thickness crack grows to the ultimate critical size (Fig. 16a, c, and e).

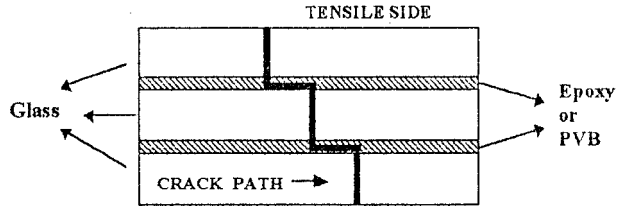

Figure 17 Schematic of the failure process in the present GPMLC samples.

The entire failure process of GPMLC as conjectured above is presented schematically in Fig. 17. To develop a simplistic picture of the sequence of failure events in the GPMLC samples, it was assumed that since the interfacial polymer layer was thin; the small amount of shear stress obtained from even the flexural loading was sufficient enough to drive the delamination cracks to grow along the interface [3, 5, 6, 13].

The general observation of crack branching in the GPMLC samples (Fig. 16a–e) possibly demands separate attention. Unfortunately, the criterion for correctly assessing the onset of crack branching in a given material is far from well understood [15–16]. Even more complex is the mechanism by which the crack branching process actually takes place [17]. However, in this connection two schools of thought exist. The first one is based on the energy balance concept [15]. The second one is based on the stress intensity concept [16]. The energy balance concept [15] predicts that crack branching occurs in a given material at a characteristic value $A = \sigma_{nc}\, r_c^{0.5}$ where r_c is the distance of the crack initiation point from a point on the boundary at which place crack branching has really occurred on the fracture surface and σ_{nc} is the corresponding component of stress acting normal to the crack at that location on the boundary. However, identification of crack initiation point on a ceramic fracture surface is far from an easy task [17].

The stress intensity criterion [16], on the other hand, claims that crack branching will occur when and only when, the local stress intensity factor attains a value equal to that of the critical stress intensity factor for the given material. The outermost glass layer of the GPMLC sample is in a state of tension under the applied three-point-bend configuration of flexural loading. So the stress field at the tip of the major crack can also activate nearby sub-major flaws on the glass surface. This process may induce, along with the growth of a major crack, secondary cracks to grow also from favourably oriented flaws. It is plausible that when fine lips of fracture from two or more adjacent flaws branch out, the phenomenon of multiple crack branching may occur, Fig. 16b. Alternatively, if such fine tongues/lips of branched cracks coalesce they can again form a large, distinct macro-crack.

As such, the physical process of crack branching is believed to initiate as a fine ribbon of fracture curves out of the primary crack plane [17]. When the crack growth velocity at the tip of such fine ribbon of fracture attains a value high enough such that the local stress intensity factor magnitude is greater than the critical stress intensity factor even when the primary crack front has not moved too far from the point of branching; the phenomenon of crack branching occurs in a sustained

manner. In the case of the present GPMLC samples, the phenomenon of crack branching was a common observation possibly linked to the enhanced toughness of the composites in comparison to those of the matrix glasses [18].

5. Conclusions

The major conclusions of the present work are:

(a) A-glass (thickness 1.01 mm) and B-glass (thickness 1.17 mm) based Glass Polymer Multi-layer Composites (A- and B-GPMLC) were fabricated with and without a thin sprayed layer of kerosene between the glass layer and the reinforcing layer in the interface where the interface was either epoxy (a thermosetting resin) or polyvinyl butyral (PVB, a thermoplastic resin). All GPMLC samples showed specific failure load data much higher than those of the corresponding glass matrices. Further, one of the A-GPMLC samples eg. A(P+K) and all the B-GPMLC samples achieved failure strain values higher than those of the corresponding matrix glasses. Among the four samples A(P+K), B(E + K), B(P) and B(P+K) which exhibited MLC like stepped load-displacement behaviour in the most pronounced fashion, three samples have the polyvinyl butyral resin as one component of the phase present as the interface between the adjacent glass layers. This observation clearly suggests that the presence of a thermoplastic resin at the interface is possibly better conducive to obtaining MLC like stress strain behaviour.

(b) All three of these above mentioned samples i.e. A(P+K), B(E+K) and B(P+K) had a thin layer of kerosene intentionally introduced between the glass layer and the reinforcing polymer layer such that a weak interface is obtained. Fractographic evidence obtained in the present work suggests that more delamination cracking occurs in such samples.

(c) The samples A(E) and B(P) exhibit highest failure stresses and the samples A(P+K) and B(P+K) show highest failure strain amongst the A- and B-GPMLC materials. All GPMLC samples taken together, the highest failure stress and strain data were obtained for A(E) and B(P+K) samples.

(d) The interfacial layer thickness (h_i) and the interfacial shear stress (τ_{xy}) can have significant influence on the specific failure load and the failure stress of the current glass polymer multi-layer composites.

Acknowledgements

One of us (AS) thanks the Department of Science and Technology (DST), Government of India, for financial help received in the form of a senior research fellowship. Project Sponsorship by DST is gratefully acknowledged by AKM. Thanks are due to Dr. Mrs. M. Chaudhury of Central Glass and Ceramic Research Institute, Calcutta for helps in Optical Microscopy.

References

1. R. MOON, K. BOCOMAN and K. TRUMBLE, *J. Amer. Ceram. Soc.* **83** (2000) 445.
2. G. ZHANG, X. YUE and T. WATANABE, *J. Euro. Ceram. Soc.* **19** (1999) 2111.
3. A. J. PHILLIPS, W. J. CLEGG and T. W. CLYNE, *Acta. Metall. Mater.* **41** (1993) 819.
4. K. HIRAO, M. E. BIRITO, P. M. TORIYAMA and S. KANZAKI, *J. Amer. Ceram. Soc.* **83** (2000) 2305.
5. J. R. MAWDSLEY, D. KOVAR and J. W. HALLORAN, *ibid.* **83** (2000) 802.
6. C. A. FOLSOM, F. W. ZOK and F. F. LAUGE, *ibid.* **77** (1994) 689.
7. *Idem.*, *ibid.* **77** (1994) 2081.
8. A. SEAL, N. R. BOSE, S. K. DALUI, A. K. MUKHOPADHYAY, K. K. PHANI and H. S. MAITI, *Bull. Mater. Sci.* **24** (2001) 101.
9. A. SEAL, S. K. DALUI, A. K. MUKHOPADHYAY, K. K. PHANI and H. S. MAITI, Paper presented in "Indo-Japan Workshop on Advanced Fibres and Composites," Sardar Patel University, Gujarat, December 6–7 (1999).
10. *Idem.*, Paper presented in "Symposium on Ceramic Matrix Composite Materials," Sardar Patel University, Gujarat, December 8–9 (1999).
11. S. TIMOSHENKO, in "Strength of Materials," 3rd edn. (D. Van Nostrand Company, Princeton, NJ, 1955) p. 92.
12. G. R. ANSTIS, P. CHAUTIKUL, B. R. LAWN and D. B. MARSHALL, *J. Amer. Ceram. Soc.* **64** (1981) 533.
13. A. J. PHILLIPPS, W. J. CLEGG and T. W. CLYNE, *Acta. Metall. Mater.* **41**(3) (1993) 805.
14. I. M. LOW and Y. W. MAI, in "Handbook of Ceramics and Composites, Vol. 2—Mechanical Properties and Speciality Applications," edited by N. P. Cheremisinoff (Marcel Dekker, New York, 1992) p. 105.
15. J. W. JOHNSON and D. G. HOLLOWAY, *Phil. Mag.* **14** (1966) 731.
16. J. CONGLETON and N. J. PETCH, *ibid.* **16** (1967) 749.
17. E. K. BEAUCHAMP, in "Fractography of Glass and Ceramics III," edited by J. R. Varmer, V. R. Frechette and G. D. Quinn, Vol. 64: Ceramic Transactions (The American Ceramic Society, OH, 1996) p. 409.
18. A. SEAL, S. K. DALUI, A. K. MUKHOPADHYAY, K. K. PHANI and H. S. MAITI, Unpublished work (2001).

Received 26 April 2001
and accepted 16 October 2002